Linear/Nonlinear Active Disturbance Rejection Switching Control for Permanent Magnet Synchronous Motors

Zhengjie Hao, Yang Yang, Yimin Gong, Zhengqiang Hao, Chenchen Zhang, Hongda Song, and Jiannan Zhang

***Abstract*—A linear/nonlinear active disturbance rejection control (ADRC) switching control (SADRC) strategy for permanent magnet synchronous motors (PMSMs) is proposed in this article to integrate the merits of the linear ADRC (LADRC) and nonlinear ADRC (NLADRC), and handle the trouble in parameter tuning and stability analysis of the NLADRC. The advantages and disadvantages of the LADRC and NLADRC are analyzed theoretically and a hysteretic switching strategy is presented to estimate and compensate the total disturbance smoothly and precisely. Based on the proposed control strategy, the SADRC controller of the PMSM is designed to achieve the accurate and robust speed control of the PMSM. Moreover, a parameter tuning strategy of the SADRC is proposed as well to simplify the parameter tuning of the NLADRC linked inextricably with that of the LADRC due to limitation of the switching conditions. Finally, the feasibility and superiority of the proposed control strategy are demonstrated on a 180 W PMSM platform.**

***Index Terms*—Active disturbance rejection control (ADRC), linear/nonlinear ADRC switching control (SADRC), parameter tuning strategy, permanent magnet synchronous motor (PMSM).**

Nomenclature

ADRC	Active disturbance rejection control.
SADRC	Linear/nonlinear ADRC switching control.
PMSM	Permanent magnet synchronous motor.
LADRC	Linear ADRC.
NLADRC	Nonlinear ADRC.
IM	Induction motor.
ESO	Extended state observer.
IMC	Internal model control.
ACO	Ant colony optimization.
APSO	Adaptive particle swarm optimization.
TD	Tracking differentiator.
SEF	State error feedback control law.
NLESO	Nonlinear ESO.
LESO	Linear ESO.
NLSEF	Nonlinear SEF.
LSEF	Linear SEF.
MPTC	Model predictive torque control.

Manuscript received September 24, 2020; revised December 18, 2020; accepted January 24, 2021. Date of publication January 27, 2021; date of current version May 5, 2021. This work was supported in part by the Engineering Laboratory Project of Jilin Provincial Development and Reform Commission under Grant 3D5204383411. Recommended for publication by Associate Editor R. Kennel. *(Corresponding author: Yang Yang.)*

Zhengjie Hao, Yang Yang, Yimin Gong, Chenchen Zhang, Hongda Song, and Jiannan Zhang are with the College of Physics, Jilin University, Changchun 130012, China (e-mail: haozj_jlu@163.com; jlu_yang@jlu.edu.cn; gongym@jlu.edu.cn; zhangcc_jlu@163.com; songhongda_jlu@163.com; zhjn@jlu.edu.cn).

Zhengqiang Hao is with the College of Communication Engineering, Jilin University, Changchun 130012, China (e-mail: haozq_jlu@163.com).

Color versions of one or more figures in this article are available at https://doi.org/10.1109/TPEL.2021.3055143.

Digital Object Identifier 10.1109/TPEL.2021.3055143

I. Introduction

PMSMs have been widely utilized in modern ac servo system with the advantages of small size, simple structure, high power density, high reliability, and convenient maintenance, especially in the fields with demanding motor performance and control accuracy such as robot, aerospace, and numerical control machines [1]–[3]. The dual closed-loop structure is adopted in the PMSM with the current loop as inner loop and the speed loop as outer loop, and the linear control like PI control method is mostly used to control the PMSM. However, the PMSM is a typical nonlinear multivariable coupling system, especially as a servo motor influenced by unknown load, motor parameter variation and magnetic field nonlinearity [4], so that the linear control is difficult to satisfy with the request of high control performance. With the rapid development of power electronic technology, microelectronics technology, and digital signal processing technology, the modern control theory and novel motor control strategy can be realized. Some modern nonlinear control algorithms have been applied to PMSM control recently, such as adaptive control method [5]–[7], sliding mode control method [8]–[10], artificial intelligence control method [11], [12], model predictive control method [13]–[16], ADRC, and so on, which not only enrich the control theory of the PMSM, but also improve the control performance of the PMSM in every respect.

The ADRC is a new nonlinear algorithm applied to the motor control in recent years and has been widely concerned in virtue of the excellent anti-disturbance ability independent of the precise system model. The ADRC technique is presented as a new control strategy first in [17], which is in the basis of nonlinear control mechanisms. The theoretical framework and experimental application of the ADRC to linear IMs are presented in [18], in which the nonlinear transformation of the state is not calculated via the IM model, but estimated online. The MPTC based on the ADRC for IMs is proposed in [19] to realize the optimal control of dynamic performance and torque tracking deviation

compensation. In comparison with the PI-MPTC, this control strategy is superior in the dynamic and steady-state performance, and possesses higher robustness. A novel sliding-mode current control strategy founded on the ADRC is presented in [20] for the PMSM to ameliorate the dynamic performance of the current controllers subjected to the internal disturbances like parameter variations. In [21], the control loops of rotor flux and speed for IMs based on the ADRC are designed to tackle both internal and external disturbances, which are estimated and compensated in virtue of two linear ESOs. And a sliding-mode component is constructed taking into consideration disturbance estimation errors and uncertainties of the control gains. An ADRC strategy for the angular speed trajectory tracking on a PMSM with serious disturbance is presented in [22]. The high-gain generalized proportional integral observer-based ADRC controller is designed to handle with the presence of unknown, time-varying load-torque inputs and system parameters. In [23], a novel robust control strategy utilizing three first-order ADRC controllers is proposed for the speed control of IMs to cope with internal and external disturbances with simple implementation and short runtime.

Moreover, owing to high sensitivity of the sensorless control to motor parameters, the ADRC is also applicable for the sensorless control of motors in virtue of high robustness to motor parameters. A speed estimation scheme for IMs in the basis of the ADRC is presented in [24], which can achieve precise disturbance estimation without the knowledge of accurate motor parameters. A novel sensorless field-oriented control strategy based on the enhanced LADRC for the PMSM is presented in [25], which the total disturbance is estimated as a feed forward compensation term of the current loop to enhance the speed estimation ability. The sensorless control of interior PMSMs based on the LADRC is proposed in [26], which obviously decreases the phase delay as well as velocity fluctuation and achieves strong anti-disturbance ability. An enhanced LADRC based HF pulse voltage signal injection scheme is presented in [27]. The cascaded ESO and linear control rules are utilized to realize the opportune and precise estimation and compensation of the whole disturbance, which improves the control performance of the PMSM subjected to disturbances. In [28], an ADRC-based sensorless control strategy for interior PMSM is presented to enhance the robustness of the speed observation adopting an ESO and a nonlinear error feedback controller for the estimation and compensation of the total disturbance. However, although the ADRC possesses the excellent performance, the systematic tuning principle of the ADRC parameters is deficient so that the LADRC with relatively easier parameter tuning is applied more widely. Therefore, it is truly essential to research on the parameter tuning method of the ADRC. A new LADRC in the basis of IMC laws and ESO is presented in [29] for superior performance of servo motors with input delay. The IMC is utilized to adjust the parameters of the LADRC according to a given set-point tracking and the ESO is adopted to estimate and compensate total disturbance founded on a nominal model. The ADRC of IMs in the basis of an APSO algorithm is presented in [30] to achieve the accurate decoupling of IMs and disturbance compensation, which adopts the APSO to tune automatically the parameters of the ADRC. The ADRC of IMs on the foundation of an ACO algorithm is presented in [31], which utilizes the ACO to adjust automatically the ADRC parameters.

In order to bring into full play the superiority of the LADRC and NLADRC, a novel PMSM control method based on the SADRC is presented in the article and the corresponding parameter tuning scheme is introduced as well. The SADRC possesses the advantages of the LADRC and NLADRC, and overcomes the shortcomings of them by means of a hysteretic switching strategy, which can realize high robustness and precision in the whole operating range. The rest of the article is organized as follows. Section II elaborates the principles and characteristics of the LADRC and NLADRC, and the SADRC is obtained on this basis. Section III introduces the designed SADRC controller for the second-order PMSM control system. In Section IV, the physical meaning and setting direction of the SADRC parameters are summarized by comparing and analyzing the influence of parameter variations on system performance, with the assistance of the frequency domain method and substantial system simulation. Section V reveals the experimental results with a 180 W PMSM drive platform, which demonstrates the feasibility and effectiveness of the proposed method. Finally, the conclusion is drawn in Section VI.

II. SADRC Control Law

The SADRC is comprised of the TD, ESO, and SEF. Taking the second-order system as an example, the system equation can be written as follows:

$$\ddot{y} = a_0 \dot{x} + a_1 x + bu + w \tag{1}$$

where y is the output variable of the system; x is the control state variable of the system; u is the input variable of the system; w is the state variable of the external disturbance; a_0 and a_1 are the unknown system parameters; and b is the control gain of the system. It can be observed from (1) that in addition to the external disturbance, the system is subjected to the internal disturbance as well stemming from the variation of system parameters. Therefore, (1) can be rewritten as follows:

$$\ddot{y} = f(x, w) + b_0 u \tag{2}$$

where b_0 is the evaluation of b; $f(x, w)$ represents the whole disturbance of the system composed of the internal and external disturbances, and can be defined as follows:

$$f(x, w) = a_0 \dot{x} + a_1 x + (b - b_0) u + w. \tag{3}$$

Then the state equation of the second-order system can be written as follows:

$$\begin{cases} \dot{x_1} = x_2 \\ \dot{x_2} = x_3 + b_0 u \\ \dot{x_3} = \dot{f}(x, w) \\ y = x_1. \end{cases} \tag{4}$$

The second-order SADRC controller can be designed according to (4).

The input variable of the system is positively related to the system error. If the initial error is big, the input variable will

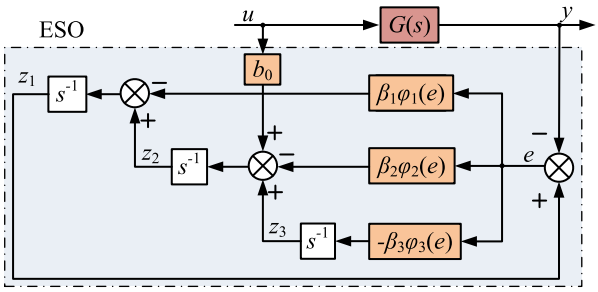

Fig. 1. Block diagram of the ESO.

become so large that it can have an adverse impact on the system control. To cope with this problem, the SADRC adopts TD to arrange a transition process for the system reference so that the actual control variable can follow the transition process to alleviate the contradictory between the overshoot and fast response. Meanwhile, the approximate differential signal of the reference can be obtained by TD. TD is a relatively independent section in the SADRC, which is not the distinction between the LADRC and NLADRC. For the sake of tracking the reference quickly, the second order TD is constructed as follows:

$$\begin{cases} \dot{\nu}_1 = \nu_2 \\ \dot{\nu}_2 = fhan\left(\nu_1 - \nu, \nu_2, r, h\right) \end{cases} \tag{5}$$

where v_1 is the tracking value of the reference; v_2 is the differential signal of the reference; ν is the reference; r is speed factor and h is the control step; and $fhan(x_1, x_2, r, h)$ is the optimal control synthesis function defined as follows:

$$\begin{cases} d = rh^2, a_0 = hx_2, y = x_1 + a_0, a_1 = \sqrt{d\left(d + 8\left|y\right|\right)} \\ a_2 = a_0 + \text{sign}\left(y\right)\left(a_1 - d\right)/2 \\ a_3 = \left(\text{sign}\left(y + d\right) - \text{sign}\left(y - d\right)\right)/2 \\ a_4 = \left(a_0 + y - a_2\right)a_3 + a_2 \\ a_5 = \left(\text{sign}\left(a_4 + d\right) - \text{sign}\left(a_4 - d\right)\right)/2 \\ fhan\left(x_1, x_2, r, h\right) = -r\left(\frac{a_4}{d} - \text{sign}\left(a_4\right)\right)a_5 - r\text{sign}\left(a_4\right). \end{cases} \tag{6}$$

ESO is the core of the SADRC, which is utilized to estimate the state variable and total disturbance $f(x, w)$ of the system. Consequently, the operation characteristics of the ESO have a significant influence on the control performance of the SADRC. The ESO of the second-order SADRC is designed as follows:

$$\begin{cases} e = z_1 - y \\ \dot{z}_1 = z_2 - \beta_1\varphi_1\left(e\right) \\ \dot{z}_2 = z_3 - \beta_2\varphi_2\left(e\right) + b_0u \\ \dot{z}_3 = -\beta_3\varphi_3\left(e\right) \end{cases} \tag{7}$$

where z_1 and z_2 are state variables of the ESO to track state variables of the system; z_3 is the state variable to track the total disturbance $f(x, w)$; β_1, β_2, and β_3 are the gains of the ESO, and $\varphi_1(e)$, $\varphi_2(e)$, and $\varphi_3(e)$ are the processing functions of the observation error. The structure of the ESO based on (7) is revealed in Fig. 1, where $G(s)$ is the mathematical model of the system. If $\varphi_1(e)$, $\varphi_2(e)$, $\varphi_3(e)$ are chosen as nonlinear functions, the ESO can be called as an NLESO. The form of a general nonlinear function is expressed as follows:

$$\varphi_i\left(e\right) = fal\left(e, \alpha_i, \delta\right) = \begin{cases} \frac{e}{\delta^{1-\alpha_i}} & \left|e\right| \le \delta \\ \left|e\right|^{\alpha_i}\text{sgn}\left(e\right) & \left|e\right| > \delta \end{cases} \tag{8}$$

where α_i and δ are undetermined parameters. When α_i<1, the function has the features of small gain with large error and large gain with small error; δ represents the linear range, aiming at avoiding the oscillation caused by the large gain of extremely small error. $\varphi_1(e)$, $\varphi_2(e)$, and $\varphi_3(e)$ can also be simply chosen as e, and in this way, the ESO can be called as an LESO.

By means of theoretical analysis and simulation research, the features of the LESO and NLESO are summarized as follows, respectively. The parameters setting and theoretical analysis of the LESO are relatively easier, and the disturbance tracking performance hardly changes with the disturbance amplitude so that the LESO is very popular in practical application; the NLESO has the advantages of better tracking performance and higher control accuracy on the premise of the same noise amplification effect as the LESO, but the parameter setting of the NLESO is relatively more complicated. Moreover, the tracking performance of the NLESO is associated with the disturbance amplitude, and that is the reason estimation capability to large disturbance of the NLESO is limited.

In view of the characteristics of the LESO and NLESO, an idea comes into existence that the LESO is operated with the large disturbance while it is switched to the NLESO with the small disturbance, which makes full use of the merits of the LESO and NLESO. Consequently, the LESO/NLESO switching strategy is introduced in the following.

When ESO tracking deviation $|e| > 1$ is satisfied, the ESO is switched to the LESO described as follows:

$$\begin{cases} e = z_1 - y \\ \dot{z}_1 = z_2 - \beta_1'e \\ \dot{z}_2 = z_3 - \beta_2'e + b_0u \\ \dot{z}_3 = -\beta_3'e \end{cases} \tag{9}$$

where β_1', β_2', and β_3' are the gains of the corresponding LESO. On the contrary, if the above condition is unsatisfied, then the ESO is switched to the NLESO expressed as follows:

$$\begin{cases} e = z_1 - y \\ \dot{z}_1 = z_2 - \beta_1 fal\left(e, \alpha_1, \delta\right) \\ \dot{z}_2 = z_3 - \beta_2 fal\left(e, \alpha_2, \delta\right) + b_0u \\ \dot{z}_3 = -\beta_3 fal\left(e, \alpha_3, \delta\right) \end{cases} \tag{10}$$

where u is set as follows:

$$u = u_0 - \frac{z_3}{b_0} \tag{11}$$

where u_0 is the output variable of the SEF which can be divided into NLSEF and LSEF, the general forms of which can be denoted as follows:

$$u_0 = \sum_{i=1}^{n} k_i fal\left(\nu_i - z_i, \alpha_i', \delta'\right) \tag{12}$$

$$u_0 = \sum_{i=1}^{n} k_i'\left(\nu_i - z_i\right) \tag{13}$$

where k_i and k_i' are the gains of NLSEF and LSEF, respectively; and α_i' and $\delta'$are two undetermined parameters of the NLSEF. When $\alpha_i'<1$, the SEF becomes an NLSEF, which possesses the features of relatively high efficiency, fast error attenuation, and high robustness. However, relatively complex parameter setting, laborious stability analysis and consecutive oscillation of small-signal place restrictions on the development of the NLSEF in practical application so that the LSEF is still mostly applied nowadays. In order to take full advantage of the NLSEF, the LSEF/NLSEF switching strategy is proposed in the following.

When either ESO tracking deviation $|e|>1$ or $|z_3|>D$ is satisfied, the SEF is switched to the LSEF described as follows:

$$u_0 = k_1' (\nu_1 - z_1) + k_2' (\nu_2 - z_2). \tag{14}$$

On the contrary, if both of the above conditions are unsatisfied, then SEF is switched to the NLSEF expressed as follows:

$$u_0 = k_1 fal (\nu_1 - z_1, \alpha_1', \delta') + k_2 fal (\nu_2 - z_2, \alpha_2', \delta'). \tag{15}$$

D is determined by the requirement of system state variables and the control range of the NLSEF is positively related to *D*. The above switching conditions of LSEF/NLSEF contain the switching conditions of LESO/NLESO so that in this article the LSEF/NLSEF switching conditions are unified as the whole switching conditions, which brings benefit to ameliorate the stability and control performance.

The general idea of the SADRC is that the LADRC is adopted to quickly track the reference in the initial stage, and then the NLADRC is utilized to enhance the tracking accuracy and anti-jamming capability; once the tracking or observation deviation gets large, the controller ought to be switched to the LADRC to ensure the fast response of the system.

III. Design of SADRC Controller for PMSM

The control object in the article is a surface-mounted PMSM with equal *d*- and *q*-axis stator inductances, the mathematical model of which is a multivariable and nonlinear system with strong coupling. Assuming that the core saturation, eddy current, and hysteresis loss are ignored as well as the symmetrical windings under the premise of guaranteed performance, the PMSM mathematical model of motion equation and voltage equation in the synchronous rotating *dq* coordinates is expressed as follows [32]:

$$\begin{cases} T_{\mathrm{e}} - T_{\mathrm{L}} = J\dot{\omega}_{\mathrm{m}} + B\omega_{\mathrm{m}} \\ T_{\mathrm{e}} = K_{\mathrm{t}} i_q = 1.5 n_{\mathrm{p}} \psi_f i_q \\ u_d = L_{\mathrm{s}} \dot{i}_d + R_{\mathrm{s}} i_d - L_{\mathrm{s}} n_{\mathrm{p}} \omega_{\mathrm{m}} i_q \\ u_q = L_{\mathrm{s}} \dot{i}_q + R_{\mathrm{s}} i_q + n_{\mathrm{p}} \omega_{\mathrm{m}} (L_{\mathrm{s}} i_d + \psi_f) \end{cases} \tag{16}$$

where T_{e} and T_{L} are electromagnetic torque and load torque, respectively; *J* is the moment of inertia; ω_{m} is the mechanical angular speed; *B* is the friction coefficient; K_{T} is the torque coefficient; i_d and i_q are the *d*- and *q*-axis currents, respectively; u_d and u_q are the *d*- and *q*-axis voltages, respectively; L_{s} and R_{s} are the stator inductance and resistance, respectively; n_{p} is the pole pairs of the PMSM; and ψ_f is the permanent magnet flux. As known from (16), there is a strong coupling relationship between i_d, i_q, and ω_{m} in the PMSM. However, due to the MTPA control of surface-mounted PMSMs, that is to say, i_d=0 control, it is unnecessary to take the coupling of i_d and i_q into account.

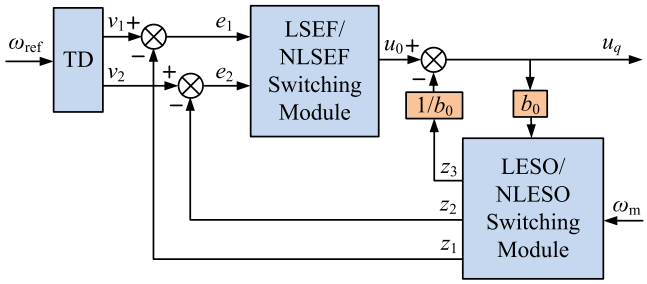

Fig. 2. Block diagram of the proposed SADRC for the PMSM.

The second-order equation of the mechanical angular velocity in PMSM can be obtained from (16) as follows:

$$\ddot{\omega}_{\mathrm{m}} = -\frac{\dot{T}_{\mathrm{L}}}{J} - \frac{B\dot{\omega}_{\mathrm{m}}}{J} - \frac{n_{\mathrm{p}} K_{\mathrm{t}} \psi_f}{J L_{\mathrm{s}}} \omega_{\mathrm{m}} - \frac{K_{\mathrm{t}} R_{\mathrm{s}}}{J L_{\mathrm{s}}} i_q + \frac{K_{\mathrm{t}}}{J L_{\mathrm{s}}} u_q. \tag{17}$$

Assuming

$$b = \frac{K_{\mathrm{t}}}{J L_{\mathrm{s}}}$$

$$f(\omega_{\mathrm{m}}, i_q, T_{\mathrm{L}}) = -\frac{\dot{T}_{\mathrm{L}}}{J} - \frac{B\dot{\omega}_{\mathrm{m}}}{J} - \frac{n_{\mathrm{p}} K_{\mathrm{t}} \psi_f}{J L_{\mathrm{s}}} \omega_{\mathrm{m}} - \frac{K_{\mathrm{t}} R_{\mathrm{s}}}{J L_{\mathrm{s}}} i_q + (b - b_0) u_q$$

then, (17) can be rewritten as follows:

$$\ddot{\omega}_{\mathrm{m}} = f(\omega_{\mathrm{m}}, i_q, T_{\mathrm{L}}) + b_0 u_q \tag{18}$$

where $f(\omega_{\mathrm{m}}, i_q, T_{\mathrm{L}})$ represents the total disturbance of the PMSM. The whole disturbance can be effectively estimated and compensated via $f(\omega_{\mathrm{m}}, i_q, T_{\mathrm{L}})$ to improve the robustness of the PMSM. The state equation of the PMSM can be expressed from (18) as follows:

$$\begin{cases} \dot{x}_1 = x_2 = \dot{\omega}_{\mathrm{m}} \\ \dot{x}_2 = x_3 + b_0 u_{\mathrm{q}} \\ \dot{x}_3 = f(\omega_{\mathrm{m}}, \dot{i}_{\mathrm{q}}, T_{\mathrm{L}}) \\ y = x_1 = \omega_{\mathrm{m}}. \end{cases} \tag{19}$$

It can be indicated that (19) is similar to (4). Therefore, each section of the SADRC controller in the PMSM can be designed according to (5), (9), (10), (11), (14), and (15), the structure of which is revealed in Fig. 2, where ω_{ref} is the reference of mechanical velocity. The SADRC controller equation of the PMSM can be expressed as follows:

$$\begin{cases} \dot{\nu}_1 = \nu_2 \\ \dot{\nu}_2 = fhan(\nu_1 - \omega_{\mathrm{ref}}, \nu_2, r, h) \\ \begin{bmatrix} \dot{z}_1 \\ \dot{z}_2 \\ \dot{z}_3 \end{bmatrix} = f_{\mathrm{ESO}} \\ u_0 = f_{\mathrm{SEF}} \\ u_q = u_0 - z_3/b_0 \end{cases} \tag{20}$$

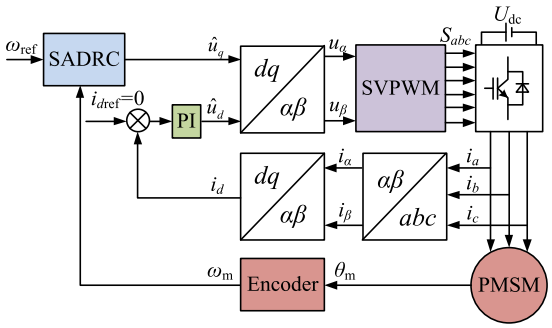

Fig. 3. Block diagram of PMSM control system based on the proposed SADRC.

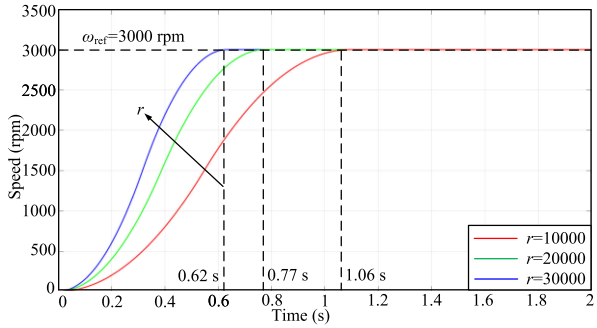

Fig. 4. Transition process tracking curves with different *r*.

where f_{ESO} is the switch between (9) and (10), and f_{SEF} is the switch between (14) and (15), in the basis of the switching conditions.

To achieve a smooth transition between the LADRC and NLADRC, a hybrid switching strategy is adopted, in which the controlled q-axis voltage $\hat{u}_q$ is obtained with the linear combination of both methods during the switch-over area, and $\hat{u}_q$ can be expressed as follows:

$$\hat{u}_q = \lambda \hat{u}_1 + (1-\lambda)\,\hat{u}_2 \tag{21}$$

$$\lambda = \frac{\alpha+\beta}{2} \tag{22}$$

$$\alpha = \begin{cases} 1 & |e| \le e_1 \\ \frac{e_2-|e|}{e_2-e_1} & e_1 < |e| < e_2 \\ 0 & |e| \ge e_2 \end{cases} \tag{23}$$

$$\beta = \begin{cases} 1 & |z_3| \le D_1 \\ \frac{D_2-|z_3|}{D_2-D_1} & D_1 < |z_3| < D_2 \\ 0 & |z_3| \ge D_2 \end{cases} \tag{24}$$

where e_1 and e_2 are the low- and up-observed speed limitation of the transition, respectively; D_1 and D_2 are the low and up observed disturbance limitation of the transition, respectively; $\hat{u}_1$ and $\hat{u}_2$ are the controlled q-axis voltage of the NLADRC and LADRC, respectively.

The controlled q-axis voltage is obtained by switching both strategies with two hysteresis bands according to (21)–(24). In order to guarantee the response and accuracy of the PMSM mechanical angular velocity, D_1 and D_2 are supposed to be set to $20\%b_0u_{q\max}$ and $25\%b_0u_{q\max}$, respectively, where $u_{q\max}$ is the maximum q-axis voltage. Moreover, e_1 and e_2 are set to 1 and 1.2, respectively, based on the characteristic of (8) which is analyzed in Section IV in detail.

The block diagram of the PMSM control system in the basis of the SADRC is shown in Fig. 3, which adopts i_d=0 control method with dual closed-loop control, namely speed loop and current loop. The SADRC controller is designed to integrate the q-axis current loop with the speed loop, forming a new speed current loop. The transition process of ω_{ref} is arranged by the TD, the differential signal of which is given as well, so that the system response is fast without overshoot. Furthermore, not only the speed and its differential value can be observed, but also the observation of total disturbance can be obtained by the LESO/NLESO switching control, such as the disturbances coming from the variation of rotational inertia, stator resistance, stator inductance, load and other unknown disturbances. Through the LSEF/NLSEF switching control, various disturbances can be compensated effectively and the nonlinear characteristics of fast response with large error and large gain with small error can be achieved. The improvement of the typical ADRC in the article also makes SADRC obtain the optimal control particularly in the case of large disturbance. The proposed SADRC strategy of the PMSM possesses the merits of the LADRC and NLADRC, and avoids the drawbacks of them via the switching strategy, which enhances the robustness and accuracy of the PMSM control. Nevertheless, the convenient parameter tuning strategy is still demanded for the SADRC to be applied in practical engineering.

IV. SADRC Parameter Tuning Strategy

The parameters of the LADRC in the SADRC controller of the PMSM can be easily tuned through the bandwidth method [33], the difficulty of which lies in the parameter tuning of the NLADRC. There is still no systematic tuning strategy for the NLADRC so far, mainly dependent on practical experience. However, the parameter tuning of the NLADRC in this article is much easier than the traditional NLADRC because the operation condition of the NLADRC proposed in the article is limited by the switching strategy. Meanwhile, the parameters of the NLADRC can be adjusted by reference to the parameters of the LADRC in the SADRC controller as well.

A. TD

The only parameter to be set in TD is speed factor *r*, which influences the tracking speed of v_1 to ω_{ref}. In order to determine the adjustment direction of *r*, the tracking curves of transition process are drawn by simulation as shown in Fig. 4, and *h*, ω_{ref} are 0.001 s and 3000 r/min, respectively. When *r* is selected as 10 000, 20 000, 30 000, the transition time is 1.06, 0.77, and 0.62 s, respectively. Hence, with the increase of *r*, v_1 reaches ω_{ref} faster, showing the better tracking performance.

B. NLESO

As known from (10), α_1, α_2, α_3, β_1, β_2, β_3, and δ are all the parameters to be set. The parameter tuning method is proposed

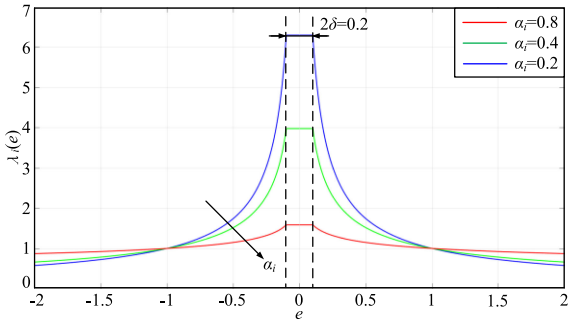

Fig. 5. Outputs of the function $\lambda_i(e)$ with different α_i.

in the article by revealing the internal law of NLESO parameters and adopting bandwidth method.

Let

$$\mathrm{fal}\left(e,\alpha_i,\delta\right)=\frac{\mathrm{fal}\left(e,\alpha_i,\delta\right)}{e}e=\lambda_i\left(e\right)e \tag{25}$$

where $i=1,2,3$. Substituting (25) into (10) yields the following:

$$\begin{cases} e=z_1-y \\ \dot{z}_1=z_2-\beta_1\lambda_1\left(e\right)e \\ \dot{z}_2=z_3-\beta_2\lambda_2\left(e\right)e+b_0u \\ \dot{z}_3=-\beta_3\lambda_3\left(e\right)e \end{cases}. \tag{26}$$

The features of the function $\lambda_i(e)$ are analyzed in the following. The functions $\lambda_i(e)$ with different α_i are compared in aspect of output variation by selecting α_i as 0.2, 0.4, and 0.8, respectively, and δ is set to 0.1, the function curves of which are shown in Fig. 5. As known in Fig. 5, with the decrease of α_i, the nonlinear degree of $\lambda_i(e)$ becomes higher and the maximum gain becomes larger. Hence, too small α_i may result in the high-frequency oscillation of observation, while the NLESO cannot play the advantages of fast error attenuation and strong anti-interference capability with large α_i. That is to say, α_i can significantly affect the performance of NLESO. In addition, the function $\lambda_i(e)$ is a constant if e is under the linear interval of [-δ, δ], and $(\lambda_i)_{\max}=\delta^{\alpha_i-1}$. When $|e|>\delta$, $\lambda_i(e)$ decreases with the increase of $|e|$, which realizes the small gain with large error and large gain with small error. For the LESO/NLESO switching control method, when $|e|>1$, $\lambda_i(e)<1$, namely relatively small gain, so e_1 and e_2 are set to 1 and 1.2, respectively, which are appropriate to be selected as the switching thresholds.

According to (26), the NLESO can be considered as a LESO with variable parameter, the parameter of which is $\beta_i\lambda_i(e)$. Thus, the parameters of the NLESO can be adjusted by adopting the bandwidth method of the LESO. First, the parameters of the LESO are adjusted taking the sampling step length, noise, etc., into account synthetically. Then, the bandwidth of the observer is set to ω_0, and correspondingly the gain of the LESO is obtained as β_i'. On the basis of Routh stability criterion, the convergence condition of the LESO is expressed as follows:

$$\beta_1'\beta_2'>\beta_3'. \tag{27}$$

As the NLESO is equivalent to the LESO with variable parameter, the convergence condition of the NLESO can be obtained as follows:

$$\beta_1\beta_2(\lambda_1\left(e\right))_{\min}(\lambda_2\left(e\right))_{\min}>\beta_3(\lambda_3\left(e\right))_{\max}. \tag{28}$$

Due to the restriction of the SADRC switching conditions, it can be obtained that

$$\left(\lambda_1\left(e\right)\right)_{\min}=\left(\lambda_2\left(e\right)\right)_{\min}=1 \tag{29}$$

$$\left(\lambda_3\left(e\right)\right)_{\max}=\delta^{\alpha_3-1}. \tag{30}$$

Substituting (29) and (30) into (28) attains the following:

$$\beta_1\beta_2>\beta_3\delta^{\alpha_3-1}. \tag{31}$$

It can be obtained that (31) is the basic principle of the NLESO parameter tuning, which not only takes into consideration the system performance, but also guarantees the system stability. As known in Fig. 5, too large linear interval δ brings about the failure of the nonlinear gain, while too small δ makes the observer more volatile. Generally, δ should be under the interval of [0.01, 0.1], and $\delta=0.03$ is suitable in this article; α_i is supposed to meet the condition of $\alpha_1>\alpha_2>\alpha_3$, and α_1, α_2, α_3 can be selected as the empirical value of 1, 0.5, 0.2, and 5 respectively.

According to the principle of the SADRC, the LESO is utilized to estimate and compensate the relatively larger disturbance, while the NLESO is only used to estimate the relatively smaller disturbance. Thus, the influences of sampling step length and noise are the key to setting parameters β_1, β_2, and β_3. Although the optimal property is enhanced with the appropriate increase of β_3, the overshoot and oscillation of the total disturbance observation can be introduced easily, which makes the PMSM stability deteriorate, and too small β_3 can limit the response of the NLESO to the disturbance as well. Hence, based on the optimal parameter setting obtained by the simulation in [34], the tuning formulas of β_1, β_2, β_3 proposed in the article are expressed as follows:

$$\beta_1=3\omega_0,\quad \beta_2=\frac{3{\omega_0}^2}{5},\quad \beta_3=\frac{{\omega_0}^3}{10}. \tag{32}$$

Substituting the tuned parameters β_1, β_2, β_3, α_3, and δ into (31) attains the following:

$$1.8{\omega_0}^3>1.4{\omega_0}^3. \tag{33}$$

It can be found that (33) is always satisfied for any ω_0 greater than zero, and thus these tuned parameters meet the stability requirement of the NLESO, which reflects the validity of the switching conditions as well. However, the steady-state and dynamic performances of the NLESO are still affected by the different ω_0. The transfer function of the disturbance observation z_3 can be written as follows [34]:

$$z_3=\frac{\lambda_2\left(e\right)\beta_3s^2\omega_{\mathrm{m}}-\lambda_3\left(e\right)\beta_3b_0u_{\mathrm{q}}}{s^3+\lambda_1\left(e\right)\beta_1s^2+\lambda_2\left(e\right)\beta_2s+\lambda_3\left(e\right)\beta_3}. \tag{34}$$

As known in (34), the NLESO has an excellent ability to suppress the disturbance of u_q, so the noise introduced by ω_{m} is the major factor of influence on the performance of the observer. Consequently, to simplify the analysis, the effects of the u_q disturbance and nonlinear function are ignored, that is to say, $u_q=0$, $\lambda_1(e)=\lambda_2(e)=\lambda_3(e)=1$ and (32) are substituted into

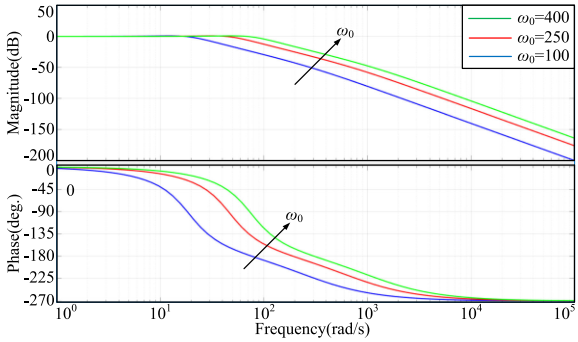

Fig. 6. Frequency analyses of the estimated disturbance with different ω_0.

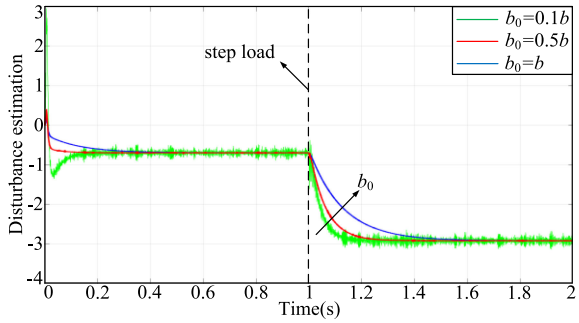

Fig. 7. Disturbance estimations with different b_0 under the step load at 1 s.

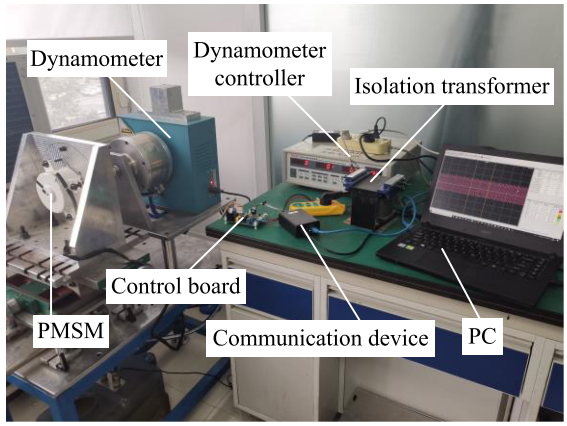

Fig. 8. Experimental setup for evaluations.

(34), and (34) can be rewritten as follows:

$$\frac{z_3}{\omega_{\mathrm{m}}} = \frac{0.1\omega_0^3 s^2}{s^3 + 3\omega_0 s^2 + 0.6\omega_0^2 s + 0.1\omega_0^3}. \tag{35}$$

The frequency domain characteristics of the estimated disturbance are shown in Fig. 6, selecting ω_0 as 100, 250, 400, respectively. With the increase of ω_0, the dynamic performance of the NLESO becomes better, which specifically reflects in the accurate estimated disturbance, small phase lag of the disturbance observation and fast convergence speed of the estimated error. However, the effect of large ω_0 to high-frequency noise is supposed not to be ignored, which leads to the deterioration of the PMSM performance. Therefore, ω_0 should be adjusted from small to large in practice until the disturbance observation satisfies the requirement of the system.

C. NLSEF

As known in (15), k_1, k_2, α_1', α_2', $\delta'$are all the parameters to be set. First, the parameters k_1', k_2' of the LSEF can be tuned, and it can be seen from (14) that they are similar to the proportional gain k_{p} and differential gain k_{d} in the PD control so that k_1', k_2' can be set as k_{p}, k_{d}, respectively, according to the parameter tuning strategy of the PD control. With regard to the NLSEF, the physical meanings of k_1, k_2 are the same as k_1', k_2' of the LSEF. Thus, k_1=k_1', k_2=k_2' and they can also be slightly adjusted nearby. The adjustment principle of α_1', α_2', δ' is similar with that of α_i and δ in the NLESO. Although the error attenuation speed becomes faster and the antijamming ability becomes stronger with the decrease of α_1', α_2', the high-frequency vibration of u_q is introduced easily as well, which brings adverse effects on the PMSM. It is generally required that $\alpha_1' \leq \alpha_2'$ for the NLSEF of the PMSM because relatively larger differential gain in PMSM controller is easy to bring about speed oscillation, so α_1', α_2', δ' are selected as 0.5, 0.75, 0.03, respectively, in this article.

D. Control Gain Estimation b_0

The core of the SADRC is to achieve the precise estimation and reasonable compensation of the whole disturbance in the PMSM control system. The control gain estimation b_0 in (18) reflects the compensation intensity of the SADRC controller. Considering the uncertainty of the model, variety of the actual operation conditions and perturbation of the motor parameters, the practical control gain of the PMSM also changes in real time. Consequently, it is essential to set the parameter b_0 reasonably in practical engineering application.

As shown in (17), the deviation of the control gain estimation b_0 can be incorporated within the total disturbance so that b_0 has the feature of strong robustness which can be adjusted in large range and guarantee the system stability. For the sake of designing the SADRC controller conveniently, b_0 can be taken as the control gain b calculated via the PMSM model and then the other parameters can be set first. After accomplishing the tuning of the other parameters, b_0 can be adjusted properly, which has influence on the dynamic performance of the PMSM. The total disturbance estimations z_3 are shown in Fig. 7 with the step load at 1 s, and b_0 is selected as $0.1b$, $0.5b$, and b, respectively. With the diminution of b_0, the disturbance compensation response becomes faster, improving the dynamic performance of the system. However, too small b_0 can bring about the overshoot and intense oscillation of the disturbance observation. Consequently, b_0 is set as $0.5b$ in the article.

V. Experimental Results

A. Experimental Setup

In order to further validate the effectiveness and superiority of the proposed SADRC controller for the PMSM, the proposed control strategy and the control strategies for comparison, including LADRC, NLADRC, PI control methods, are implemented in a 180-W PMSM setup, shown in Fig. 8, and the

TABLE I
PARAMETERS OF THE PMSM PROTOTYPE

Symbol	Quantity	Value
n_p	Number of pole-pairs	3
K_t	Torque coefficient	0.625 N·m/A
R_s	Stator resistance	3.2 Ω
L_s	Stator inductance	54.6 mH
ω_N	Rated speed	3000 rpm
T_N	Rated torque	0.48 N·m
I_N	Rated current	0.8 A
P_N	Rated power	180 W
V_{dc}	DC-link voltage	310 V

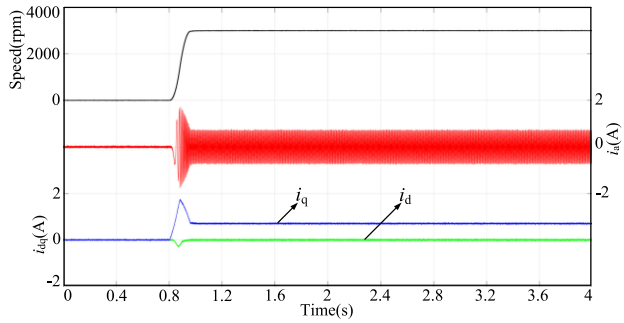

Fig. 9. Start-up performance of the PMSM based on the SADRC.

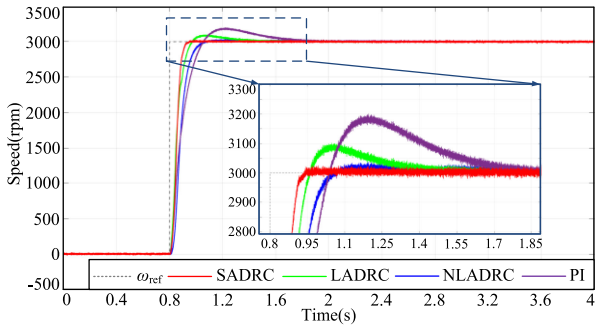

Fig. 10. Start-up performance comparison of the PMSM.

main parameters of the PMSM prototype are listed in Table I. In this setup, a mechanically coupled load dynamometer is employed to generate the load torque. The control algorithms are executed by a STM32F301C8T6 MCU with the control frequency of 8 kHz and the PMSM is driven by an intelligent power module STGIPQ5C60T with the switching frequency of 8 kHz. A quadrature encoder is installed at the end of the shaft to measure the speed of the PMSM prototype. Furthermore, the parameters of the SADRC, LADRC, and NLADRC are the same in view of the parameter tuning strategy in Section IV. The parameter r of the TD is 5×10^4, and the SADRC, LADRC, and NLADRC are of the same gains, which are set as $k_1=k_1'=7.34$, $k_2=k_2'=3.2$, $\beta_1=\beta_1'=1.5\times10^3$, $\beta_2=\beta_2'=1.5\times10^5$, $\beta_3=\beta_3'=1.25\times10^7$, and the other parameters of the SADRC is tuned as $\alpha_1=1, \alpha_2=0.5, \alpha_3=0.25, \alpha_1'=0.5, \alpha_2'=0.75, \delta=\delta'=0.03$, and $b_0=3200$, which is the same as the NLADRC. The speed loop parameters of the PI control method are chosen as $k_{sp}=1.344$, $k_{si}=0.27$, and the current loop parameters are corrected as $k_{cp}=27.3$, $k_{ci}=1600$ with the same bandwidth of the SADRC based on the frequency domain method [35].

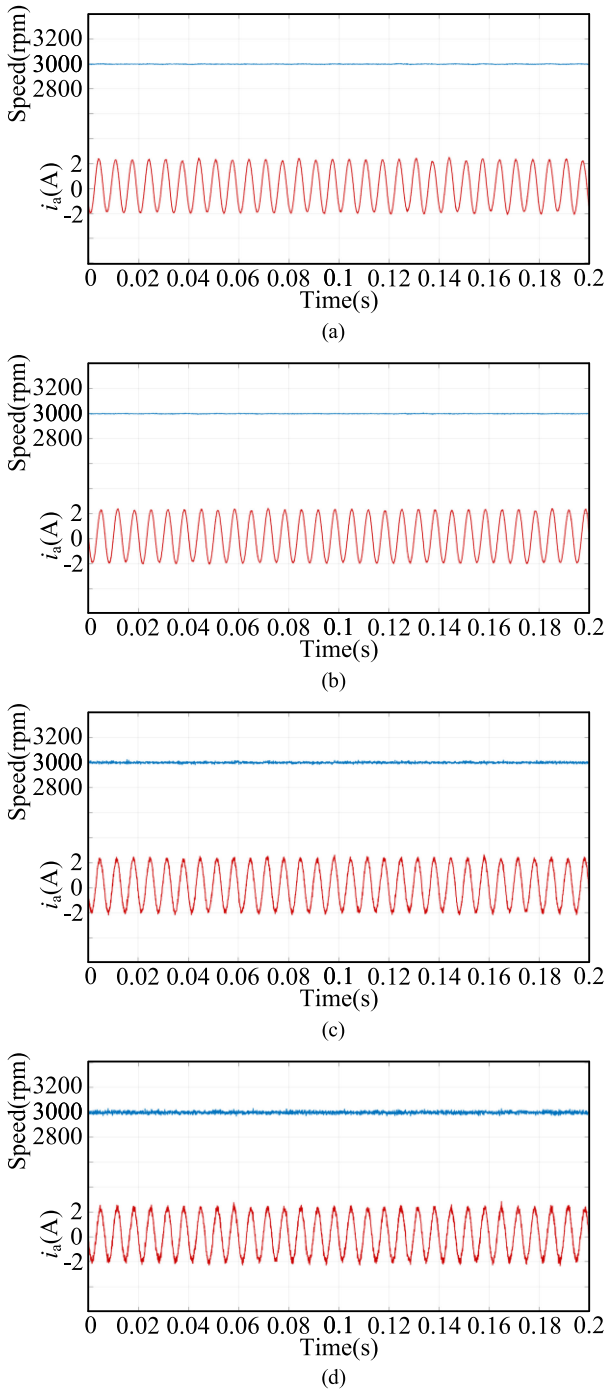

Fig. 11. Steady-state performances at given state. (a) SADRC. (b) NLADRC. (c) LADRC. (d) PI.

B. Start-Up Performance

The first experimental test is the comparative experiment of the PMSM start-up performance. The waveforms of the speed, phase current i_a, d- and q-axis currents in the PMSM based on the SADRC are revealed in Fig. 9, the reference speed of which is set to 3000 r/min. After the arrangement of the speed transition

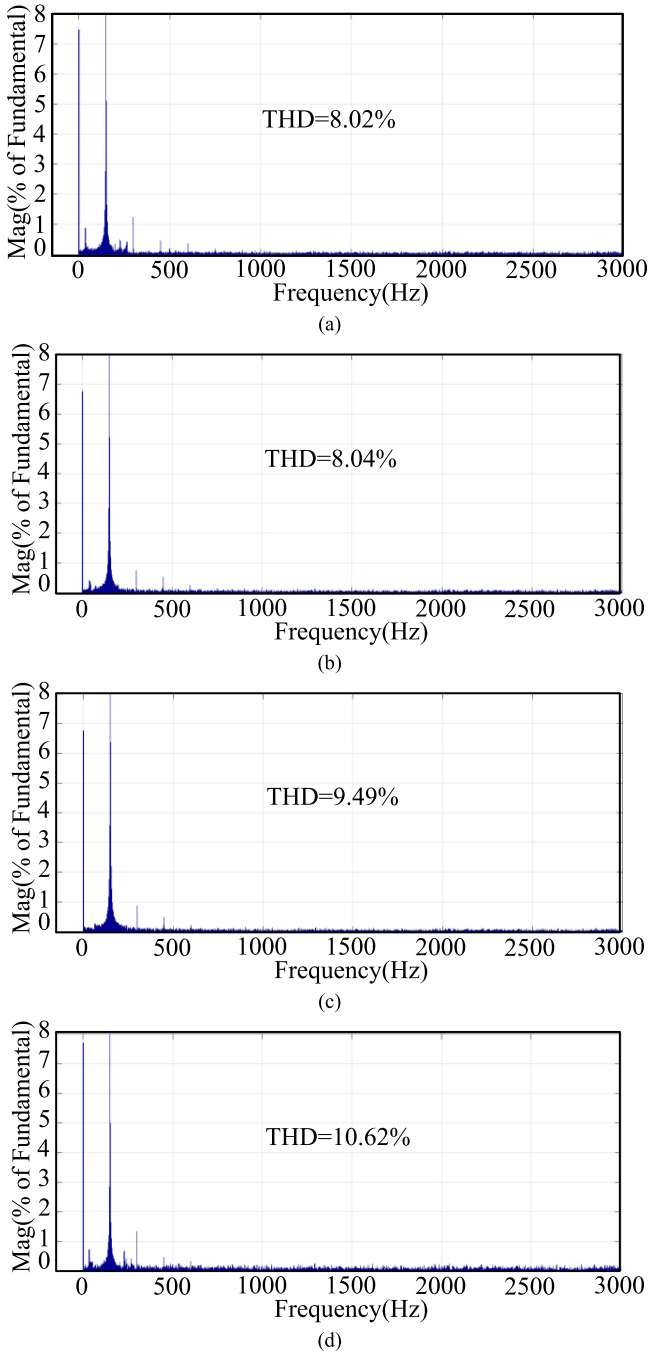

Fig. 12. Steady-state stator current harmonic of the PMSM at given state. (a) SADRC. (b) NLADRC. (c) LADRC. (d) PI.

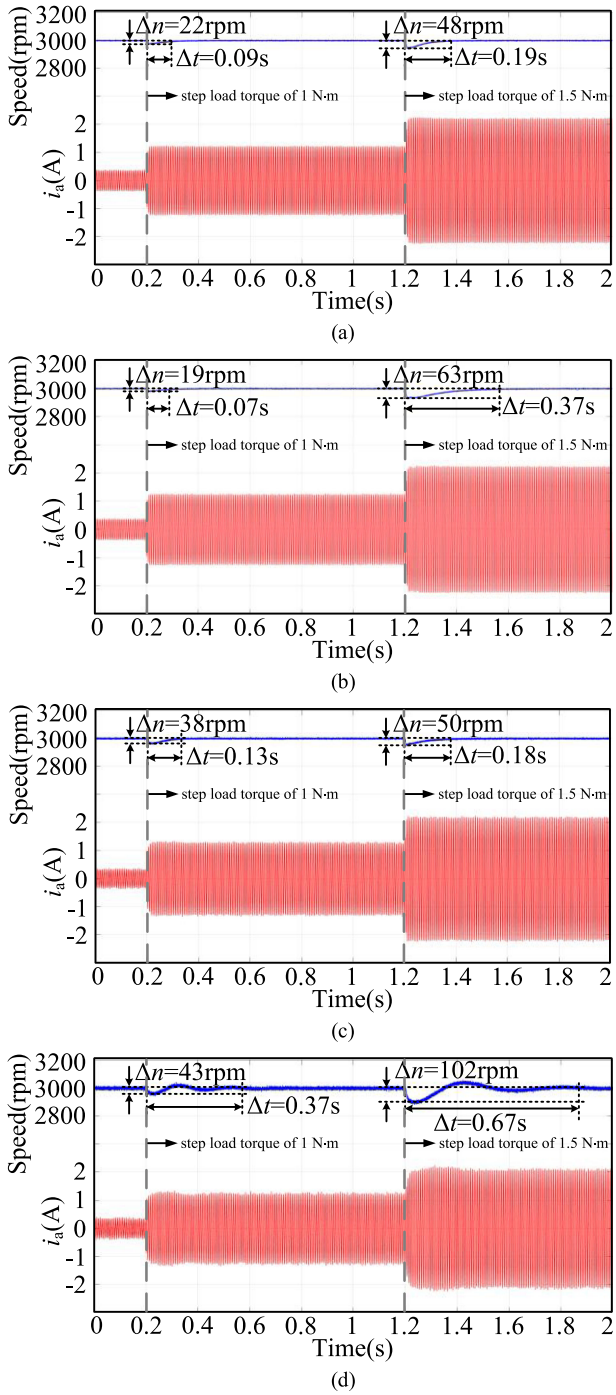

Fig. 13. Dynamic performances at 3000 rpm under step load torque of 1 and 1.5 N·m. (a) SADRC. (b) NLADRC. (c) LADRC. (d) PI.

process in advance by the TD, the actual speed can track the set speed rapidly without the speed overshoot and overcurrent, which demonstrates the excellent start-up performance of the proposed SADRC.

The start-up performance comparison between the SADRC, LADRC, NLADRC, and PI control strategies is revealed in Fig. 10, and the comparative results are shown in Table II, where σ is the speed overshoot and t_s is the settling time. It can be obviously seen that the speed overshoot and settling time of the PI control strategy are relatively larger and longer, while the start-up performances of the SADRC, LADRC, and NLADRC

TABLE II
START-UP PERFORMANCE COMPARISON OF THE PMSM

Performance metrics	SADRC	LADRC	NLADRC	PI
σ (rpm)	11	91	17	179
t_s (s)	0.21	0.69	0.46	1.05

are relatively better. More specifically, the speed regulation of the LADRC with the large speed difference is rapid so that the actual speed can reach the target speed quickly, but a certain of speed overshoot is generated and the settling time is correspondingly

TABLE III
DYNAMIC PERFORMANCE COMPARISON OF THE PMSM

Performance metrics		3000/1500/100/0 rpm			
		SADRC	NLADRC	LADRC	PI
Δn (rpm)	1 N·m	22/25 /24/21	19/25 /22/21	38/34 /35/32	43/39 /45/41
	1.5 N·m	48/44 /47/49	63/61 /68/71	50/46 /49/47	102/94 /98/91
Δt (s)	1 N·m	0.09/0.07 /0.1/0.11	0.07/0.11 /0.08/0.13	0.13/0.12 /0.15/0.14	0.37/0.32 /0.33/0.3
	1.5 N·m	0.19/0.17 /0.18/0.2	0.37/0.35 /0.39/0.4	0.18/0.17 /0.2/0.19	0.67/0.56 /0.59/0.63

prolonged due to the poor speed regulation capacity of the LADRC under the circumstance of small speed difference. On the contrary, the speed regulation of the NLADRC with the large speed difference is relatively slower, but the strong speed regulation ability of the NLADRC has the effect of alleviating the speed overshoot. The proposed SADRC combines the advantages of the LADRC and NLADRC, and avoids their deficiencies, the start-up performance of which is superior to that of the LADRC and NLADRC, with tiny speed overshoot and short settling time.

C. Steady-State Performance

The second experimental test is the comparative experiment of the PMSM steady-state performance. The given speed and load torque are set to the rated value of 3000 r/min and maximum value of 1.5 N·m, respectively. The waveforms of speed as well as phase current and current harmonics of the PMSM are revealed in Figs. 11 and 12, respectively, comparing the steady-state performances of the SADRC, NLADRC, LADRC, PI control strategies. It can be seen that the speed fluctuation of the PI control method is the largest and that of the LADRC is relatively smaller, while the speed fluctuations of the NLADRC and SADRC strategies are the smallest, which can also be reflected by the current harmonics of the PMSM shown as Fig. 12. The current harmonics of the PMSM adopting SADRC, NLADRC, LADRC, PI control strategies are 8.02%, 8.04%, 9.49%, 10.62%, respectively, which demonstrates the superior steady-state performance of the proposed SADRC due to same characteristic of large gain with small error as the NLADRC.

D. Dynamic Performance

The third experimental test is the comparative experiment of the PMSM dynamic performance, which is mainly reflected in the dynamic response of the motor speed under the different step load torque to highlight the distinction between the NLADRC and LADRC. Moreover, the comparative experiments at different given speeds are aimed to confirm the effectiveness and superiority of the SADRC in the whole speed range. The speed and phase current waveforms of the SADRC, NLADRC, LADRC, PI control strategies under the step load torque of 1 and 1.5 N·m at 3000, 1500, 100, and 0 r/min are revealed in Figs. 13–16, respectively. The comparative experimental results of the dynamic performance in the PMSM are summarized in Table III. This indicates clearly that the dynamic performance of

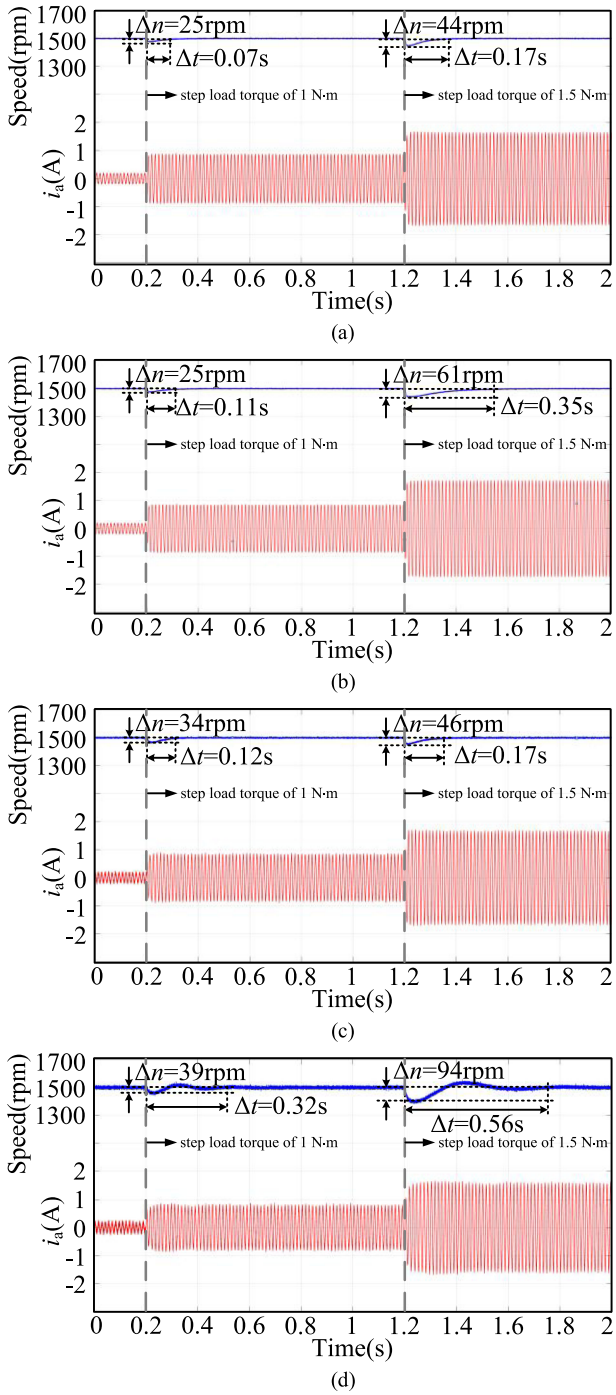

Fig. 14. Dynamic performances at 1500 rpm under step load torque of 1 and 1.5 N·m. (a) SADRC. (b) NLADRC. (c) LADRC. (d) PI.

the PMSM utilizing the ADRC is superior to that of the PMSM utilizing the PI control while the dynamic performances of the LADRC and NLADRC method both under the step load torque of 1 and 1.5 N·m are significantly different in the two circumstances. According to the theoretical analysis of the LADRC and NLADRC in Section II, the response of the LADRC to large disturbance is faster than that of the NLADRC, while the gain of the NLADRC to small disturbance is larger than that of the LADRC. Consequently, the dynamic performance of the

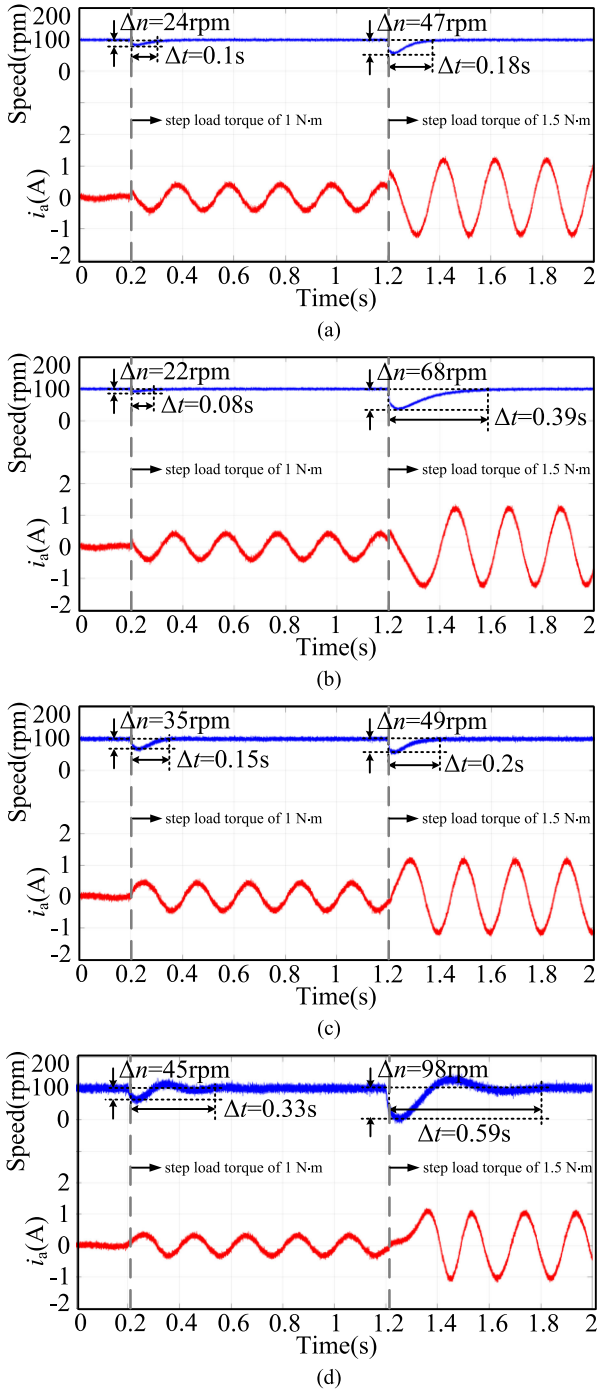

Fig. 15. Dynamic performances at 100 rpm under step load torque of 1 and 1.5 N·m. (a) SADRC. (b) NLADRC. (c) LADRC. (d) PI.

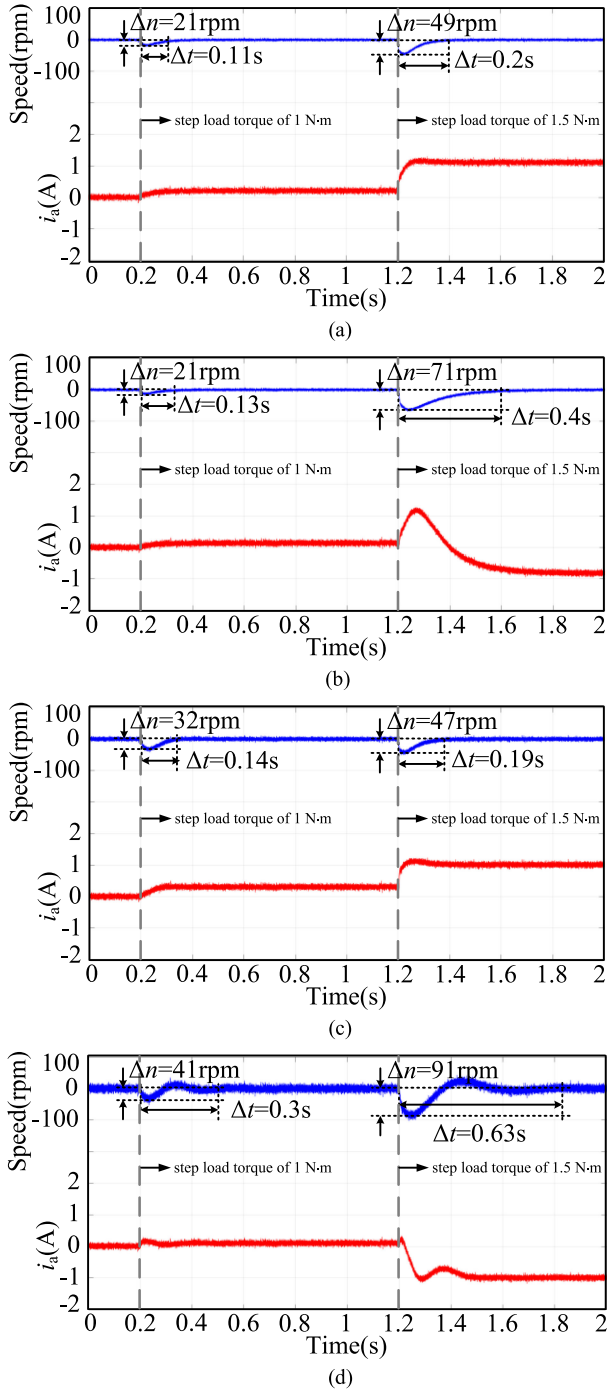

Fig. 16. Dynamic performances at 0 rpm under step load torque of 1 and 1.5 N·m. (a) SADRC. (b) NLADRC. (c) LADRC. (d) PI.

LADRC is superior to that of the NLADRC under the large step load torque, while the dynamic performance of the NLADRC is superior to that of the LADRC under the small step load torque. The SADRC proposed in the article unites the merits of the LADRC and NLADRC through the switching control strategy, which validates the better dynamic performance than that of the NLADRC, LADRC, PI control strategies under the range between 0 and 100% of step maximum load torque as shown in Fig. 17. Furthermore, Fig. 18 reveals that the speed fluctuation maximums Δn and settling times Δt of the SADRC at the speed from 0 to 3000 r/min under the same step load torque are both smaller than those of the other strategies which demonstrates that SADRC can maintain the superior dynamic performance in the whole speed.

E. Robustness to Motor Parameters

The fourth experimental test is the comparative experiment of the robustness to PMSM parameters. In the SADRC controller

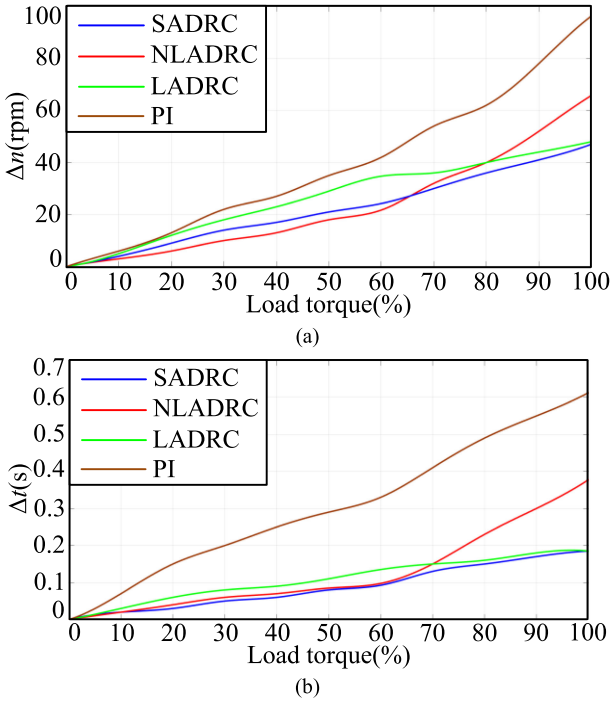

Fig. 17. Dynamic performance comparison under the range between 0% and 100% of step maximum load torque considering the influence of speed comprehensively. (a) Speed fluctuation maximum. (b) Settling time.

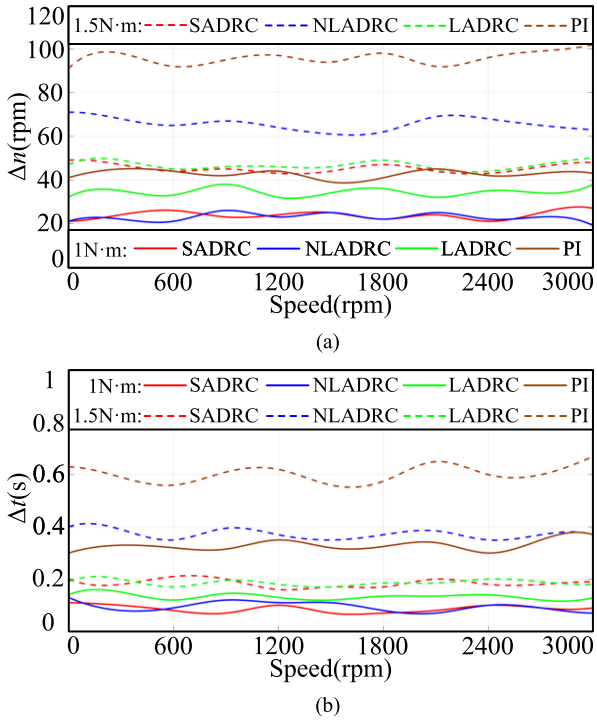

Fig. 18. Dynamic performance comparison at the speed from 0 to 3000 r/min under step load torque of 1 and 1.5 N·m. (a) Speed fluctuation maximum. (b) Settling time.

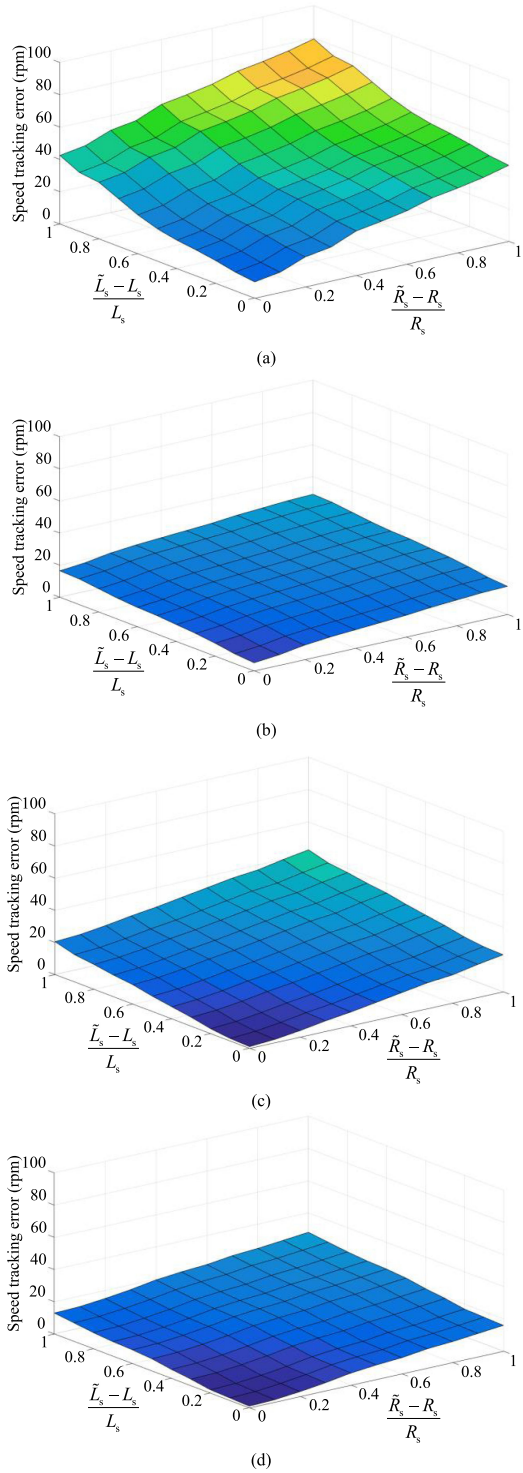

Fig. 19. Speed tracking errors when $\tilde{R}_s$ and $\tilde{L}_s$ vary in the range between 100% and 200% of R_s and L_s. (a) PI. (b) LADRC. (c) NLADRC. (d) SADRC.

of the PMSM, the mismatched parameters like stator resistance and inductance are noted as $\tilde{R}_s$ and $\tilde{L}_s$, respectively, which undergo the variation in the range between 100% and 200% of R_s and L_s in the experimental test, and corresponding results are revealed in Fig. 19. The experiment tests the speed tracking performance of the PMSM under the rated speed condition not only when the variations of $\tilde{R}_s$ and $\tilde{L}_s$ work alone, but also when they work simultaneously, and the maximum speed tracking error occurs when $\tilde{R}_s$ and $\tilde{L}_s$ change to the 200% of R_s and L_s concurrently. As shown in Fig. 19, the speed tracking error surface can clearly reflect the superiority of the ADRC in

robustness to PMSM parameters compared with the PI control strategy. In particular, the speed tracking performance of the SADRC is better than that of the LADRC with small parameter mismatch and the NLADRC with large parameter mismatch, because the SADRC possesses the features of large gain with small error and fast response with large error. Consequently, the direct comparison of SADRC, NLADRC, LADRC, and PI control methods demonstrates the higher robustness to PMSM parameters with the SADRC.

VI. Conclusion

In this article, a novel SADRC strategy for the PMSM was proposed in order to enhance the control performance of the PMSM, which possesses the LADRC feature of fast response with large error and the NLADRC feature of large gain with small error. The SADRC can maintain the ability of estimation and compensation to disturbances in different operation conditions and effectively improve the robustness and tracking accuracy of the system. Taking the nonlinear mechanism of the PMSM into account, the SADRC controller is constructed, the anti-interference mechanism of which was analyzed in depth. In particular, the influence of each parameter on the dynamic and steady-state performance of the whole system was emphatically studied, and then the rules of SADRC parameter tuning was summarized. The proposed SADRC strategy was comprehensively compared with NLADRC, LADRC, PI control strategies on a 180 W PMSM platform. The experimental results show that the SADRC strategy is superior in start-up performance, steady-state performance, and parameter sensitivity of the PMSM. In respect of the dynamic performance, the speed fluctuation maximum and settling time of the SADRC are approximately 10.7 r/min and 0.046 s smaller than those of the LADRC, respectively, under the step load torque of 1 N·m in the whole range; these metrics of the SADRC are approximately 20.2 r/min and 0.188 s smaller than those of the NLADRC, respectively, under the step load torque of 1.5 N·m as well. Hence, the effectiveness and feasibility of the SADRC for the PMSM is verified, which is especially applicable for variable parameter systems.

References

[1] J. Lara, J. Xu, and A. Chandra, "Effects of rotor position error in the performance of field-oriented-controlled PMSM drives for electric vehicle traction applications," *IEEE Trans. Ind. Electron.*, vol. 63, no. 8, pp. 4738–4751, Aug. 2016.

[2] X. Zhou, J. Sun, H. Li, and X. Song, "High performance three-phase PMSM open-phase fault-tolerant method based on reference frame transformation," *IEEE Trans. Ind. Electron.*, vol. 66, no. 10, pp. 7571–7580, Oct. 2019.

[3] Y. C. Kwon, S. K. Sul, N. A. Baloch, S. Morimoto, and M. Ohto, "Design, modeling, and control of an IPMSM with an asymmetric rotor and search coils for absolute position sensorless drive," *IEEE Trans. Ind. Appl.*, vol. 52, no. 5, pp. 3839–3850, Sep./Oct. 2016.

[4] F. Bu *et al.*, "Speed ripple reduction of direct-drive PMSM servo at low-speed operation using virtual cogging torque control method," *IEEE Trans. Ind. Electron.*, vol. 68, no. 1, pp. 160–174, Jan. 2021.

[5] A. K. Junejo, W. Xu, C. Mu, M. M. Ismail, and Y. Liu, "Adaptive speed control of PMSM drive system based a new sliding-mode reaching law," *IEEE Trans. Power Electron.*, vol. 35, no. 11, pp. 12110–12121, Nov. 2020.

[6] L. Wang, Z. Q. Zhu, H. Bin, and L. M. Gong, "Current harmonics suppression strategy for PMSM with nonsinusoidal back-EMF based on adaptive linear neuron method," *IEEE Trans. Ind. Electron.*, vol. 67, no. 11, pp. 9164–9173, Nov. 2020.

[7] M. L. Masmoudi, E. Etien, S. Moreau, and A. Sakout, "Amplification of single mechanical fault signatures using full adaptive PMSM observer," *IEEE Trans. Ind. Electron.*, vol. 64, no. 1, pp. 615–623, Jan. 2017.

[8] C. Gong, Y. Hu, J. Gao, Y. Wang, and L. Yan, "An improved delay-suppressed sliding-mode observer for sensorless vector-controlled PMSM," *IEEE Trans. Ind. Electron.*, vol. 67, no. 7, pp. 5913–5923, Jul. 2020.

[9] Y. Wang, Y. Feng, X. Zhang, and J. Liang, "A new reaching law for antidisturbance sliding-mode control of PMSM speed regulation system," *IEEE Trans. Power Electron.*, vol. 35, no. 4, pp. 4117–4126, Apr. 2020.

[10] V. Repecho, D. Biel, and A. Arias, "Fixed switching period discrete-time sliding mode current control of a PMSM," *IEEE Trans. Ind. Electron.*, vol. 65, no. 3, pp. 2039–2048, Mar. 2018.

[11] D. Flieller, N. K. Nguyen, P. Wira, G. Sturtzer, D. O. Abdeslam, and J. Mercklé, "A self-learning solution for torque ripple reduction for nonsinusoidal permanent-magnet motor drives based on artificial neural networks," *IEEE Trans. Ind. Electron.*, vol. 61, no. 2, pp. 655–666, Feb. 2014.

[12] H. Yan, Y. Xu, F. Cai, H. Zhang, W. Zhao, and C. Gerada, "PWM-VSI fault diagnosis for a PMSM drive based on the fuzzy logic approach," *IEEE Trans. Power Electron.*, vol. 34, no. 1, pp. 759–768, Jan. 2019.

[13] G. Wu, S. Huang, Q. Wu, F. Rong, C. Zhang, and W. Liao, "Robust predictive torque control of N∗3-phase PMSM for high-power traction application," *IEEE Trans. Power Electron.*, vol. 35, no. 10, pp. 10799–10809, Oct. 2020.

[14] Y. Zhou and G. Chen, "Predictive DTC strategy with fault-tolerant function for six-phase and three-phase PMSM series-connected drive system," *IEEE Trans. Ind. Electron.*, vol. 65, no. 11, pp. 9101–9112, Nov. 2018.

[15] T. Türker, U. Buyukkeles, and A. F. Bakan, "A robust predictive current controller for PMSM drives," *IEEE Trans. Ind. Electron.*, vol. 63, no. 6, pp. 3906–3914, Jun. 2016.

[16] J. Hang, J. Zhang, M. Xia, S. Ding, and W. Hua, "Interturn fault diagnosis for model-predictive-controlled-PMSM based on cost function and wavelet transform," *IEEE Trans. Power Electron.*, vol. 35, no. 6, pp. 6405–6418, Jun. 2020.

[17] J. Han, "Auto-disturbance-rejection controller and its application," *Control Decis.*, vol. 13, no. 1, pp. 19–23, Jan. 1998.

[18] F. Alonge, M. Cirrincione, F. D'lppolito, M. Pucci, and A. Sferlazza, "Active disturbance rejection control of linear induction motor," *IEEE Trans. Ind. Appl.*, vol. 53, no. 5, pp. 4460–4471, Oct. 2017.

[19] L. Yan, F. Wang, M. Dou, Z. Zhang, R. Kennel, and J. Rodríguez, "Active disturbance-rejection-based speed control in model predictive control for induction machines," *IEEE Trans. Ind. Electron.*, vol. 67, no. 4, pp. 2574–2584, Apr. 2020.

[20] L. Qu, W. Qiao, and L. Qu, "Active-disturbance-rejection-based sliding-mode current control for permanent-magnet synchronous motors," *IEEE Trans. Power Electron.*, vol. 36, no. 1, pp. 751–760, Jan. 2021.

[21] F. Alonge, M. Cirrincione, F. D'lppolito, M. Pucci, and A. Sferlazza, "Robust active disturbance rejection control of induction motor systems based on additional sliding-mode component," *IEEE Trans. Ind. Electron.*, vol. 64, no. 7, pp. 5608–5621, Jul. 2017.

[22] H. Sira-Ramírez, J. Linares-Flores, C. García-Rodríguez, and M. A. Contreras-Ordaz, "On the control of the permanent magnet synchronous motor: An active disturbance rejection control approach," *IEEE Trans. Control Syst. Technol.*, vol. 22, no. 5, pp. 2056–2063, Sep. 2014.

[23] J. Li, H. Ren, and Y. Zhong, "Robust speed control of induction motor drives using first-order auto-disturbance rejection controllers," *IEEE Trans. Ind. Appl.*, vol. 51, no. 1, pp. 712–720, Jan./Feb. 2015.

[24] C. Du, Z. Yin, J. Liu, Y. Zhang, and X. Sun, "A speed estimation method for induction motors based on active disturbance rejection observer," *IEEE Trans. Power Electron.*, vol. 35, no. 8, pp. 8429–8442, Aug. 2020.

[25] L. Qu, W. Qiao, and L. Qu, "An enhanced linear active disturbance rejection rotor position sensorless control for permanent magnet synchronous motors," *IEEE Trans. Power Electron.*, vol. 35, no. 6, pp. 6175–6184, Jun. 2020.

[26] B. Du, S. Wu, S. Han, and S. Cui, "Application of linear active disturbance rejection controller for sensorless control of internal permanent-magnet synchronous motor," *IEEE Trans. Ind. Electron.*, vol. 63, no. 5, pp. 3019–3027, May 2016.

[27] G. Wang, R. Liu, N. Zhao, D. Ding, and D. Xu, "Enhanced linear ADRC strategy for HF pulse voltage signal injection-based sensorless IPMSM drives," *IEEE Trans. Power Electron.*, vol. 34, no. 1, pp. 514–525, Jan. 2019.
[28] G. Zhang, G. Wang, B. Yuan, R. Liu, and D. Xu, "Active disturbance rejection control strategy for signal injection-based sensorless IPMSM drives," *IEEE Trans. Transp. Electrific.*, vol. 4, no. 1, pp. 330–339, Mar. 2018.
[29] P. Li, G. Zhu, and M. Zhang, "Linear active disturbance rejection control for servo motor systems with input delay via internal model control rules," *IEEE Trans. Ind. Electron.*, vol. 68, no. 2, pp. 1077–1086, Feb. 2021.
[30] C. Du, Z. Yin, Y. Zhang, J. Liu, X. Sun, and Y. Zhong, "Research on active disturbance rejection control with parameter autotune mechanism for induction motors based on adaptive particle swarm optimization algorithm with dynamic inertia weight," *IEEE Trans. Power Electron.*, vol. 34, no. 3, pp. 2841–2855, Mar. 2019.
[31] Z. Yin, C. Du, J. Liu, X. Sun, and Y. Zhong, "Research on autodisturbance-rejection control of induction motors based on an ant colony optimization algorithm," *IEEE Trans. Ind. Electron.*, vol. 65, no. 4, pp. 3077–3094, Apr. 2018.
[32] Z. Tang and B. Akin, "A new LMS algorithm based deadtime compensation method for PMSM FOC drives," *IEEE Trans. Ind. Appl.*, vol. 54, no. 6, pp. 6472–6484, Nov./Dec. 2018.
[33] B. Sun and Z. Gao, "A DSP-based active disturbance rejection control design for a 1-kW H-bridge DC-DC power converter," *IEEE Trans. Ind. Electron.*, vol. 52, no. 5, pp. 1271–1277, Oct. 2005.
[34] K. Li, Y. Xia, X. Qi, and Z. Gao, "On the necessity, scheme, and basis of the linear-nonlinear switching in active disturbance rejection control," *IEEE Trans. Ind. Electron.*, vol. 64, no. 2, pp. 1425–1435, Feb. 2017.
[35] K. Li, "PID tuning for optimal closed-loop performance with specified gain and phase margins," *IEEE Trans. Control Syst. Technol.*, vol. 21, no. 3, pp. 1024–1030, May 2013.

Zhengjie Hao received the B.Sc. degree in electrical engineering and automation and the M.S. degree in electrical engineering from Jiangsu University, Zhenjiang, China, in 2016 and 2019, respectively. He is currently working toward the Ph.D. degree with Jilin University, Changchun, China.

His research interests include control technology for PMSM.

Yang Yang received the Ph.D. degree from Jilin University, Changchun, China, in 2018.

He is currently a Postdoctoral Fellow with the College of Physics, Jilin University. His research interests include power electronics and control of PMSM.

Yimin Gong received the Ph.D. degree from Jilin University, Changchun, China, in 2008.

He is currently a Professor with the College of Physics, Jilin University. His current research interests include electrical machines and their control systems.

Zhengqiang Hao received the B.S. and M.S. degrees in 2016 and 2019, respectively, from Jilin University, Changchun, China, where he is currently working toward the Ph.D. degree in control science and engineering.

His research interests include optimized sensorless control in PMSM.

Chenchen Zhang received the B.S. and M.S. degrees, in 2016 and 2019, respectively, from Jilin University, Jilin, China, where he is currently working toward the Ph.D. degree in applied physics.

His research interests include power electronics, high-performance ac motor drives, and sensorless control for electrical drives.

Hongda Song received the B.S. and M.S. degrees in 2016 and 2019, respectively, from Jilin University, Changchun, China, where he is currently working toward the Ph.D. degree in applied physics.

His research interests include electrolytic capacitorless motor drives, thermal simulation, magnetic simulation, and single-phase rectifiers.

Jiannan Zhang received the B.S. and M.S. degree from Jilin University, Changchun, China, in 2014 and 2017, respectively.

She is currently an Engineer with the College of Physics, Jilin University. Her research interests include electromagnetic simulation.